STM JOURNALS

Journal of
Thin Films, Coating Science
Technology and Application

ISSN: 2455-3344
Volume 13, Issue 2, 2026
May–August
DOI (Journal): 10.37591/JoTCSTA

https://journals.stmjournals.com/jotcsta

Research JoTCSTA

Enhanced Room-Temperature Gas Sensing Performance of 2% Mn-Doped Sri Lankan Natural Graphite Thin-Film Sensors for Ammonia, Acetone, and Ethanol vapors Detection

I.G.P.N. Karunasena[1], P.G.D.C.K. Karunarathna[2], Roshan Thotagamuge[3], P. Samarasekara[4,*]

Abstract

The development of room-temperature gas sensors with high sensitivity, fast response, and low-cost remains a critical challenge for environmental monitoring and safety applications. In this work, we report the fabrication and characterization of a 2% Mn-doped Sri Lankan natural graphite thin-film sensor for the detection of ammonia (NH_3), ethanol (C_2H_5OH), and acetone (C_3H_6O) vapors under ambient conditions. The sensor was prepared using the doctor-blade coating method on Indium Tin Oxide (ITO) glass substrates, followed by thermal annealing at 100°C. Structural and morphological analyses using X-ray diffraction (XRD) and scanning electron microscopy (SEM) confirmed the successful incorporation of Mn, with an estimated porosity of 18.94%. Gas sensing measurements revealed that Mn doping significantly enhances the performance of natural graphite. The highest response was observed for C_3H_6O with a sensitivity of 36.92%, followed by NH_3 (9.77%) and C_2H_5OH (9.55%). Compared to undoped graphite, the Mn-doped sensor exhibits improved sensitivity and reduced response/recovery times, particularly showing a substantial decrease in recovery time due to enhanced adsorption-desorption kinetics. The improved sensing behavior is attributed to Mn-induced surface activation, increased defect sites, and enhanced charge transfer interaction between gas molecules and the graphite surface. The overall results demonstrate that Mn-doped Sri Lankan natural graphite is a promising low-cost material for efficient gas sensing applications. This study provides a viable pathway for developing simple, scalable, and high-performance gas sensors based on doped natural graphite systems.

***Author for Correspondence**
P. Samarasekara
E-mail: pubudus@sci.pdn.ac.lk

[1]Research Assistant, Postgraduate Institute of Science, University of Peradeniya, Peradeniya, Sri Lanka
[2]Senior lecturer, Department of Nano Science Technology, Faculty of Technology, Wayamba University of Sri Lanka, Kuliyapitiya, Sri Lanka
[3]Senior lecturer, Department of Optometry, University of Sri Jayewardenepura, Sri Lanka
[4]Senior Professor, Department of Physics, Faculty of Science, University of Peradeniya, Peradeniya, Sri Lanka

Received Date: May 18, 2026
Accepted Date: May 27, 2026
Published Date: June 17, 2026

Citation: I.G.P.N. Karunasena, P.G.D.C.K. Karunarathna, Roshan Thotagamuge, P. Samarasekara. Enhanced Room-Temperature Gas Sensing Performance of 2% Mn-Doped Sri Lankan Natural Graphite Thin-Film Sensors for Ammonia, Acetone, and Ethanol vapors Detection. Journal of Thin Films, Coating Science Technology and Application. 2026; 13(2): 39–49p.

Keywords: Doctor-blade method, Gas sensitivity, Gas sensors, Mn-doped graphite, Sri Lankan graphite, Ammonia sensing, Thin-film sensor

INTRODUCTION

Gas sensors play a critical role in environmental monitoring, industrial safety, agriculture, and human health protection by detecting harmful, toxic, and flammable gases in real time. Among various gases, NH_3, C_2H_5OH, and C_3H_6O are significant air pollutants that pose serious health risks and environmental risks in terms of chemical processes, space missions, and agricultural and medical applications. However, current solid-state gas sensing devices remain limited by insufficient sensitivity and selectivity, particularly at low gas concentrations at room-temperature. The

development of advanced doped material-based sensors capable of detecting multiple gas species with high sensitivity and fast response and recovery times remains an urgent technological necessity [1–4].

Recent investigations have demonstrated that Sri Lankan natural graphite presents considerable promise as a candidate material for next-generation gas sensors, attributed to its exceptional physical properties [5]. The two-dimensional structure of graphite confers several advantageous characteristics for gas sensing applications, including good carrier mobility, a large surface-to-volume ratio, and excellent mechanical flexibility, rendering graphite fundamentally suitable for detecting gas molecules. However, despite these advantages, Sri Lankan natural graphite faces significant limitations in practical gas sensing applications. The near-zero band gap of undoped graphite severely restricts electronic tunability, while the absence of dangling bonds on the carbon surface results in weak physisorption interactions with gas molecules.

Consequently, these weak van der Waals interactions give rise to low adsorption energies, insufficient charge transfer, prolonged response and recovery times, collectively compromising the sensor performance and practical applicability [6].

To address these limitations, recent studies have explored transition metal doping as an effective strategy for enhancing gas sensing performance. Comparative studies have demonstrated that aluminum-doped graphene exhibits significantly improved sensitivity toward CO molecule absorption relative to pristine graphene. Density functional theory (DFT) calculations further substantiate that manganese (Mn)-doped graphene exhibit enhanced stability and superior gas sensing characteristics compared to pristine graphene [7]. Recent investigations employing Spin-unrestricted DFT calculations have revealed that Mn-doped graphene subjected to external electric fields is a promising candidate for N_2O adsorptive decomposition [8].

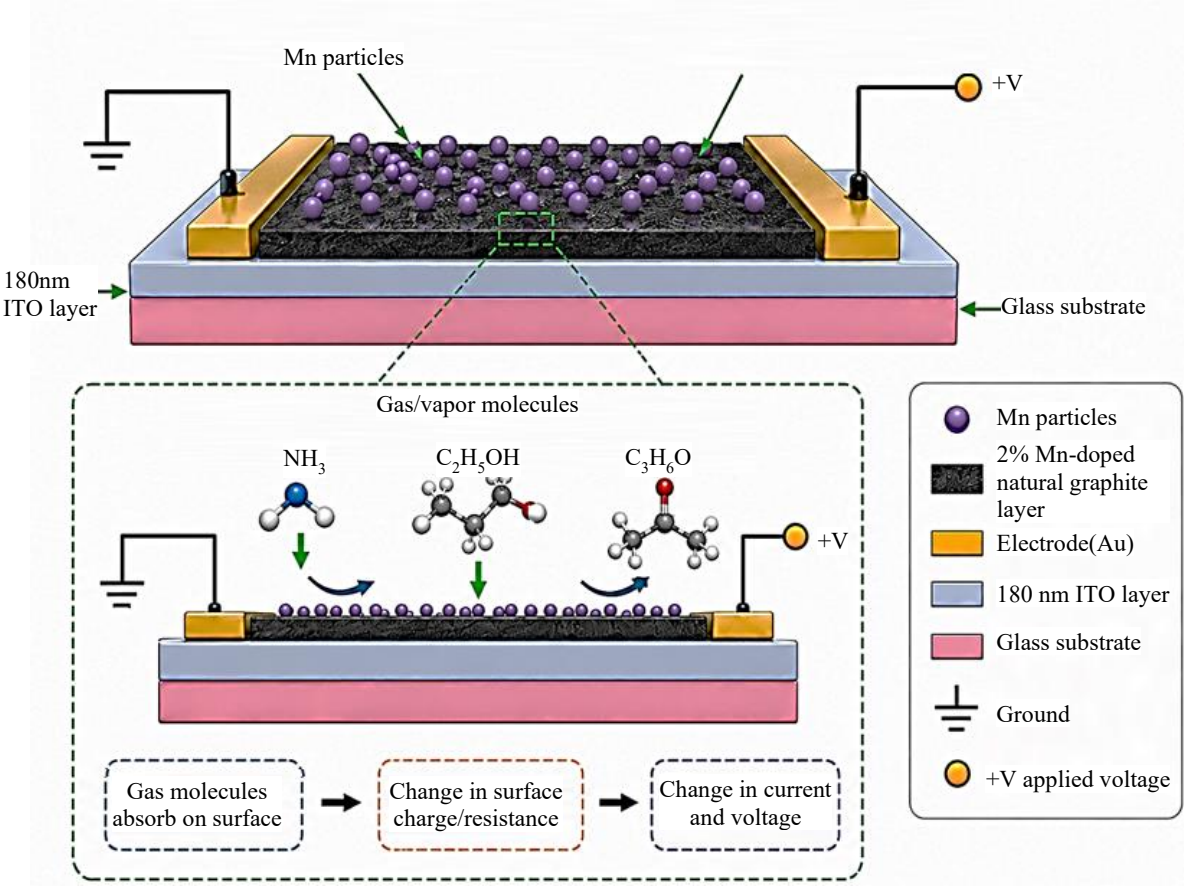

Figure 1. Schematic structure of the prepared 2% Mn-doped sensor sample.

Furthermore, emerging research has identified that Mn atoms incorporated within single vacancies (MnSV-GP) and Mn atoms coordinated with three nitrogen atoms in defective graphene structures demonstrate superior structural stability and enhanced responsive capabilities across multiple gas and vapor species, including CH_2O, CO, N_2O, S_2O, and NH_3. Notably, MnSV-GP exhibited a rapid recovery time of 1.1 s for N_2O sensing at room-temperature [9]. These findings provide a compelling foundation for the development of Mn-doped graphene-based sensors with enhanced sensitivity and practical utility.

Motivated by these advancements, this study investigates the gas sensing potential of 2% Mn-doped Sri Lankan natural graphite for detecting NH_3, C_2H_5OH, and C_3H_6O vapors under ambient conditions. The primary objective of this study is to evaluate the feasibility of fabricating cost-effective room-temperature gas sensors using doped natural graphite as the sensing material. Specifically, the key parameters influencing sensor sensitivity and response-recovery characteristics were systematically examined to design efficient graphite-based gas sensors.

EXPERIMENTAL WORK

Sample Preparation

A graphite sample (BCB20) with 99.1% carbon content was obtained from Bogala Lanka Ltd. In Sri Lanka. Following the methodology of Yi et al. (2012), graphite and 2% Mn were dispersed in a mixture of distilled water and C_3H_6O (75 wt.% C_3H_6O) to prepare a coating solution [10]. ITO glass substrates were patterned by selectively removing the conductive ITO layer at the center, thereby creating two electrically isolated regions suitable for the sensor electrode configuration. Prior to coating, the substrates were cleaned sequentially with C_3H_6O, rinsed thoroughly with distilled water, and dried afterward. The substrate resistance was measured to verify the electrical isolation between the two ITO regions. The graphite dispersion was deposited onto the ITO substrate via the doctor-blade method, as shown in Figure 1. Thermal treatment was performed at 100°C for 3 h in ambient air to facilitate the complete evaporation of water and organic solvents. The post-annealing sample resistance was measured to characterize the fabricated device.

Structural and Morphological Measurements

Graphite dispersion was deposited onto non-conductive glass substrates for structural and morphological analyses. X-ray diffraction (XRD) measurements were performed using a Rigaku Ultima IV diffractometer with CuKα radiation to determine the crystal structure and phase composition of the graphite sample. Scanning electron microscopy (SEM) analysis was performed using a Zeiss EVO LS15 SEM instrument to examine the surface morphology of the sensor.

Gas Sensitivity Measurements

The coated sensor was mounted in a sealed test chamber and contacted using gold-coated electrodes. As shown in Figure 2, the device was biased at 5 V through a series of resistors, and the voltage across the resistor was recorded. After a stabilization period of 30 min in air, 1000 ppm of the target vapor was introduced into the chamber, and the voltage response was monitored until a steady state was reached. The chamber was then flushed with ambient air to desorb the vapor while continuously recording the voltage. These measurement cycles were repeated for each vapor, and all gas sensing tests were conducted at room-temperature.

RESULTS AND DISCUSSION

XRD Characterization of the Samples

Figure 3 shows the XRD patterns of pure Mn, natural graphite, and 2% Mn-doped natural graphite samples. The XRD pattern of Mn confirms the presence of pure Mn in the sample [11]. The diffraction pattern of the undoped natural graphite sensor exhibited a prominent peak at $2\theta = 25.970°$, corresponding to the (002) plane. In contrast, the 2% Mn-doped natural graphite sample shows a

shifted peak at 2θ = 26.54° for the (002) plane. This shift in the (002) diffraction peak after Mn doping can be attributed to lattice distortion and possible intercalation effects, which alter the interlayer spacing of graphite [12, 13]. Similar shifts towards higher diffraction angles, associated with defect formation and structural modification, have been reported in intercalated graphite systems. Moreover, such peak shifts are commonly linked to the substitutional of dopant atoms and the resulting lattice strain in the host material.

For further analysis, the XRD pattern of the 2% Mn-doped natural graphite sample is presented in Figure 4. A comparison between the undoped and doped samples revealed that the pure graphite sample did not exhibit distinct peaks in the 2θ range of 25° to 60°, whereas the doped sample showed several small but clear peaks. As shown in Figure 4, the magnified view highlights these peaks more clearly, and they correspond well with the characteristic peaks observed in the pure Mn XRD pattern shown in Figure 3. This confirms the successful incorporation of Mn into a graphite matrix.

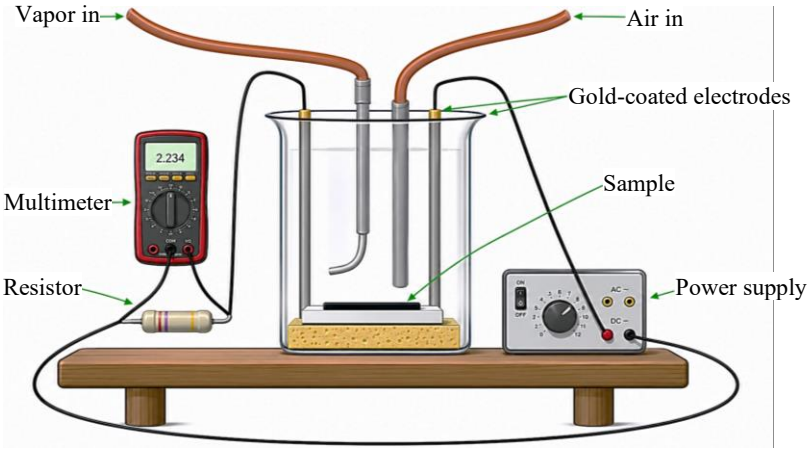

Figure 2. The experimental setup is used to measure the gas vapor response and recovery time of the sensor [5].

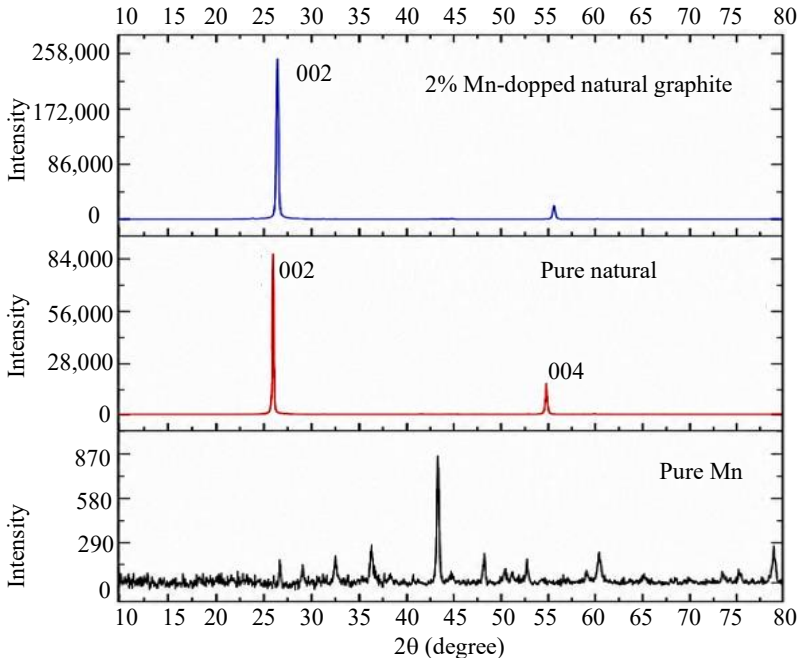

Figure 3. XRD patterns of pure Mn, natural graphite [5], and 2% Mn-doped graphite samples, showing the structural differences.

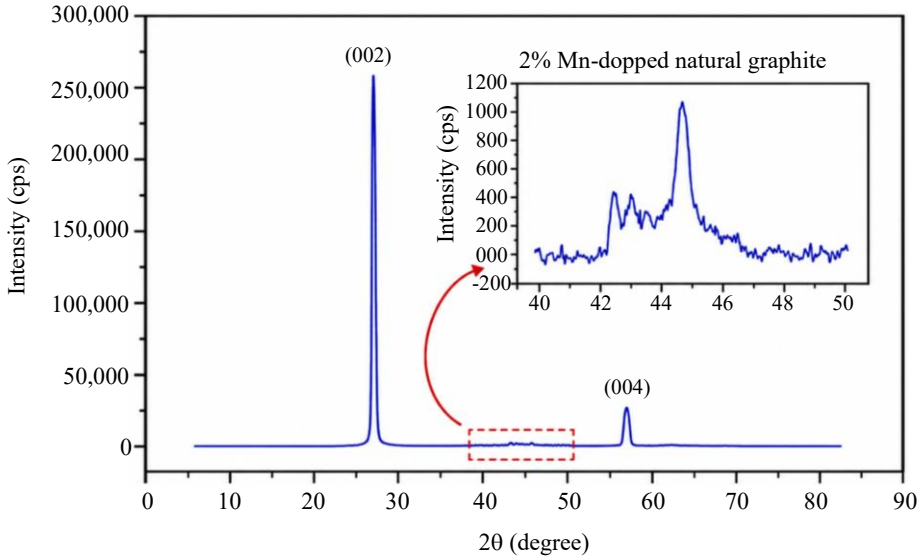

Figure 4. XRD pattern of the 2% Mn-doped natural graphite sample showing the structural features induced by Mn doping.

Table 1. Calculated values of interplanar spacing, FWHM, crystallite size, and strain for the 2% Mn-doped graphite sample.

Graphite sample	Miller indices	Diffraction angle (2θ)	Bragg angle (θ)	Interplane distance (d) (Å)	FWHM (deg)	Crystallite size (nm)	Strain ($\times 10^{-4}$)
2% Mn-doped natural graphite	(002)	26.54	13.27	3.3558	0.2598	34.92	11.03

Furthermore, the XRD pattern of the prepared thin-film closely resembled that of graphite powder, indicating the absence of any preferred crystallographic orientation. This suggests an isotropic distribution of the crystallites within the film. Several structural parameters were calculated based on the XRD data. The interplanar distance d_{00l} for the sample was calculated using Bragg's law [14, 15].

$$d_{00l} = \lambda/2\, sin\theta_{00l} \quad (1)$$

The Crystallite sizes (D) were calculated using the Scherrer equation, and the strain (ε) is given by

$$D = \frac{k\lambda}{\beta cos(\theta)} \quad (2)$$

$$\varepsilon = \frac{\beta cos(\theta)}{4} \quad (3)$$

where λ is the radiation wavelength of Cu-Kα radiation (λ =1.54060 Å), θ is the reflection angle for the reflex (00l) (l = 2, 4, or 6), β is the full width at half maximum (FWHM) of the XRD peak at angle θ; *and* k is a constant specific to the crystal direction (k = 0.9). The calculated values of the crystallite size are summarized in Table 1 [16].

Surface Morphology Analysis

Figure 5 shows the SEM images of the 2% Mn-doped natural graphite sample. The particles exhibited irregular shapes, which are characteristic of natural graphite. Owing to the van der Waals forces between the graphite layers, the particles appear densely packed, resulting in a compact structure. The porosity of the sample was calculated to be 18.94% using the ImageJ software. The presence of Mn particles can be clearly observed in Figure 5(a), confirming the successful incorporation of Mn into the graphite matrix. Figures 5(b) and 5(c) further illustrate the arrangement of the graphite particles within the sample. The particles were densely packed, which explains the relatively low porosity value obtained.

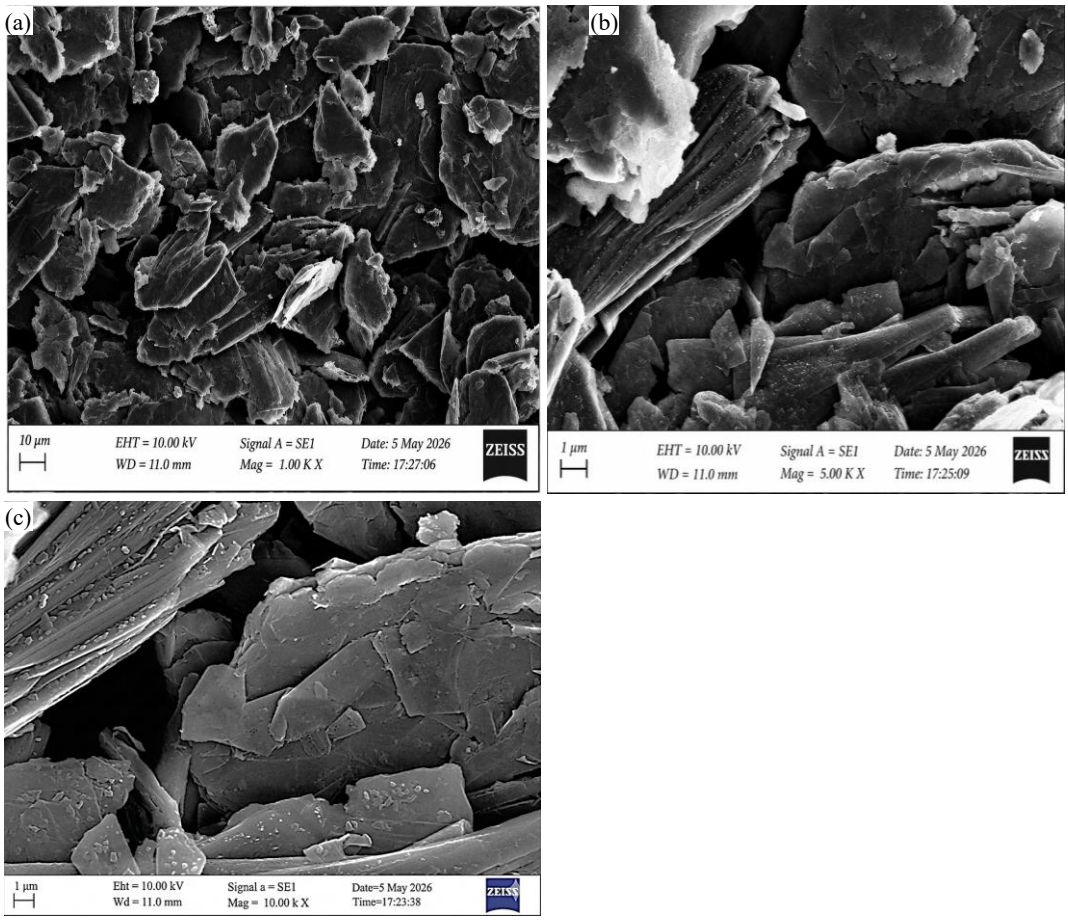

Figure 5. (a)–(c) SEM images of the thin-film graphite samples at different magnifications: (a) 1000x, (b) 5000x, and (c) 10000x.

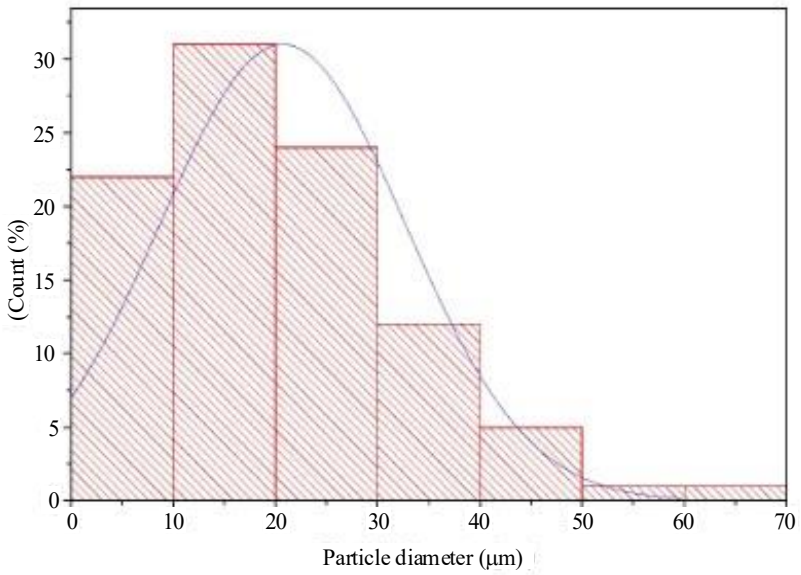

Figure 1. Particle size distribution of the thin-film graphite sample.

Particle size analysis was performed using the ImageJ software, and the corresponding distribution is presented in Figure 6. The particle diameters ranged from 4.35 to 70 µm, with the majority of particles distributed between 10 and 20 µm.

Gas Sensitivity of the Samples

The gas sensitivity of each vapor was evaluated using the following equation:

$$\text{Gas sensitivity} = \frac{|R_g - R_a|}{R_a} \times 100\% \quad (4)$$

Where,

R_a is the sensor resistance in air, and Rg is the sensor resistance in the target gas. The resistance and current were calculated using the following equations:

$$R = \left(\frac{5}{v} - 1\right) s \quad (5)$$

$$I = \left(\frac{5-v}{R}\right) \quad (6)$$

Recent studies, as shown in Figure 7(a), indicate that the natural graphite sensor exhibits the highest gas sensitivity towards C_3H_6O (23.98%), followed by C_2H_5OH (7.16%), and NH_3 (6.37%). Among these vapors, C_3H_6O also demonstrated the shortest response and recovery times (50 and 22 min, respectively). In comparison, NH_3 showed response and recovery times of 110 and 46 min, respectively, whereas C_2H_5OH exhibited 124 and 22 min, respectively [17].

The response of the 2% Mn-doped sensor, as shown in Figure 7(b), followed a trend similar to that of the natural graphite sensor. The sensor voltage increased with time as vapor was adsorbed on the sensor surface. As shown in Figure 7(b), C_3H_6O exhibits the highest gas sensitivity (36.92%) along with the shortest response and recovery times (48 and 10 min, respectively). NH_3 shows response and recovery times of 80 and 12 min, with a sensitivity of 9.77%, while C_2H_5OH shows 80 and 14 min with a sensitivity of 9.55%.

In both Figure 8(a) and 8(b), exposure to NH_3, C_2H_5OH, and C_3H_6O vapors led to an increase in the sensor voltage, accompanied by a corresponding increase in the resistance. In this configuration, the current through the sensor varies inversely with the resistance of the sensor. The increase in resistance during vapor exposure suggests the adsorption of gas molecules on the sensor surface, which may involve charge transfer interactions and possible surface oxidation processes [5].

When comparing the natural graphite sensor with the 2% Mn-doped graphite sensor, the C_3H_6O sensitivity increased from 23.98% to 36.92% upon Mn doping, indicating a significant improvement in the sensing performance. Similarly, the sensitivity towards NH_3 and C_2H_5OH increased after Mn incorporation.

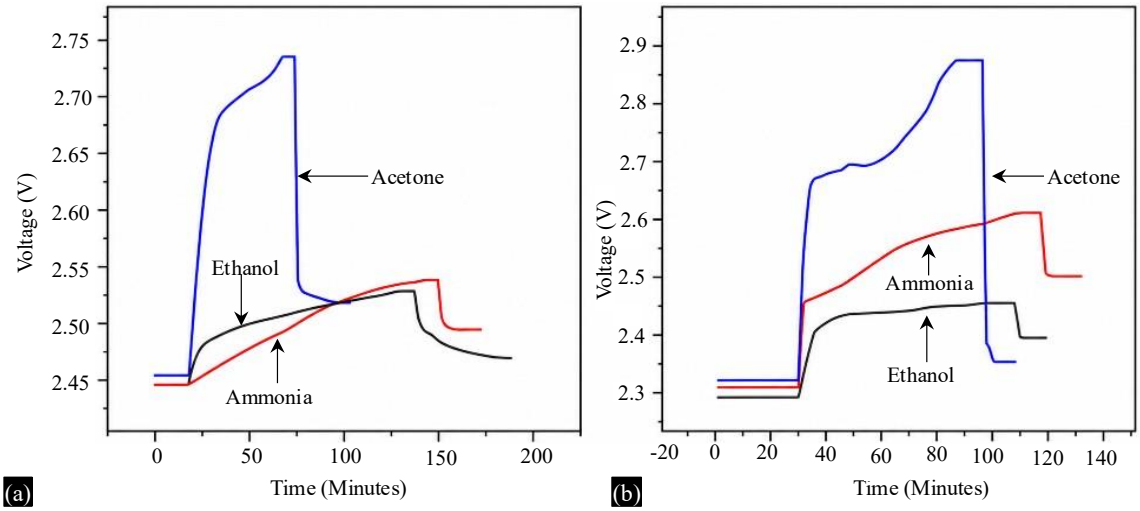

Figure 7. (a) to (b) Time-dependent voltage response of (a) the natural graphite sensor and (b) the 2% Mn-doped sensor towards NH_3, C_2H_5OH, and C_3H_6O [5].

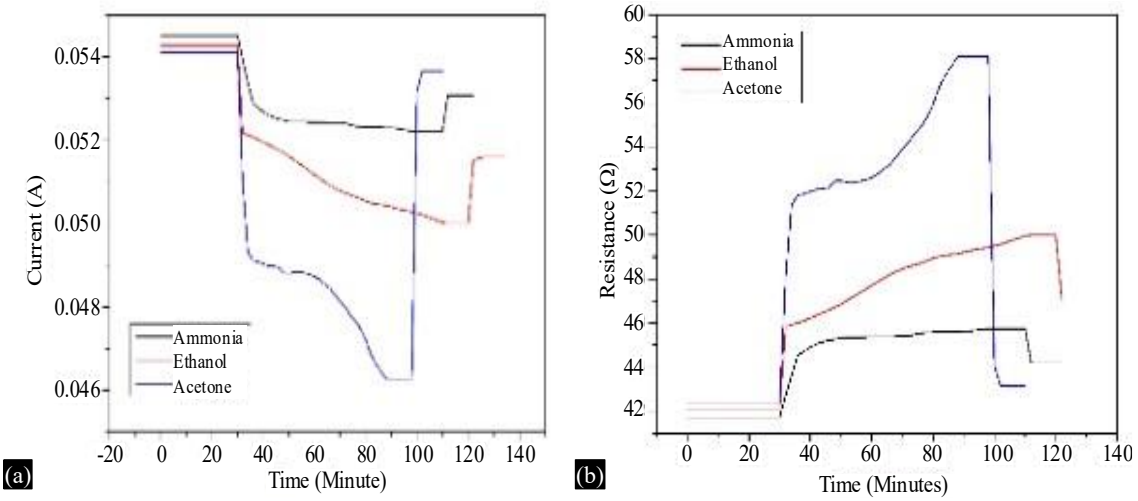

Figure 8. (a)–(b) Graphical representations of (a) current and (b) resistance of the 2% Mn-doped graphite sensor upon exposure to NH_3, C_2H_5OH, and C_3H_6O vapors.

Table 2. Compares key performance metrics between natural graphite and 2% Mn-doped sensors, highlighting substantial improvements from Mn doping.

Vapor	Metric	Natural graphite	2% Mn-Doped	Improvement (%)
C_3H_6O	Sensitivity (%)	23.98	36.92	+54
	Response (minutes)	50	48	-4
	Recovery (minutes)	22	10	-55
NH_3	Sensitivity (%)	6.37	9.77	+53
	Response (minutes)	110	80	-27
	Recovery (minutes)	46	12	-74
C_2H_5OH	Sensitivity (%)	7.16	9.55	+33
	Response (minutes)	124	82	-34
	Recovery (minutes)	22	14	-36

The response and recovery times were notably reduced for the doped sensor. For C_3H_6O, the natural graphite sensor required 50 min to reach a stable response and showed a recovery time of 22 min, whereas the 2% Mn-doped sensor exhibited response and recovery times of 48 and 10 min, respectively. Similarly, for NH_3, the response and recovery times decreased from 110 and 46 min (natural graphite sensor) to 80 and 12 min (Mn-doped sensor), respectively. C_2H_5OH also showed improved dynamics, with response and recovery times reduced from 124 and 22 min to 80 and 14 min, respectively. A summary of the performance of both the natural graphite and 2% Mn-doped graphite sensors is presented in Table 2. The observed improvement in the gas sensing performance is likely attributed to the presence of Mn, which enhances the surface-active sites and increases the adsorption capability of the sensor.

These comparative improvements suggest that Mn is an effective and cost-effective dopant for enhancing the room-temperature gas sensing performance of Sri Lankan natural graphite sensors for C_3H_6O, NH_3, and C_2H_5OH.

As illustrated in Figure 9, the three-cycle response curves obtained at 1000 ppm show that the sensor did not fully return to its initial baseline after the reintroduction of air into the chamber. Instead, the signal stabilized at a higher resistance level before gradually approaching the original baseline, indicating incomplete recovery between the cycles. This behavior can be attributed to the partial retention of vapor molecules on the sensor surface, even under air purging, leading to a gradual increase in baseline resistance in successive cycles.

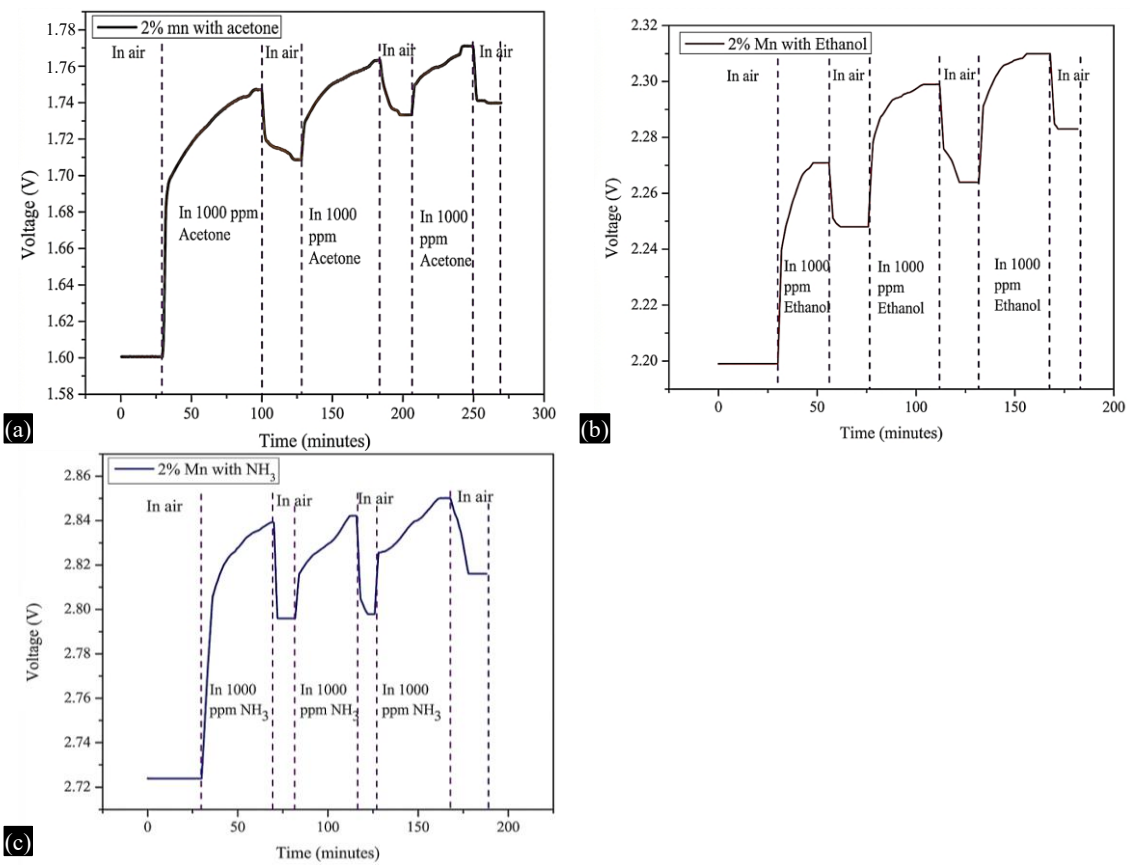

Figure 9. (a)–(c) Response and recovery characteristics of the 2% Mn-doped natural graphite sensor exposed to 1000 ppm of (a) C_3H_6O, (b) C_2H_5OH, and (c) NH_3

For C_3H_6O, a clear decline in response time was observed over repeated exposures: the response time decreased from 70 min in the first cycle to 54 min in the second cycle and further to 42 min in the third cycle. A similar decreasing trend in the response time was observed for all three vapors, suggesting that the residual adsorbed species and modified surface states from previous cycles facilitated faster adsorption and charge transfer during subsequent exposures. This progressive acceleration in the response is consistent with an adsorption-desorption mechanism, in which partial surface coverage from earlier cycles enhances the sensor activation upon re-exposure.

The gas sensing behavior is likely governed by physisorption, where vapor molecules are weakly bound to the sensor surface through van der Waals interactions, resulting in changes in resistance. Because physisorption is generally reversible, the absorbed molecules can be desorbed under reduced pressure or elevated temperature. Because the measurements in this study were performed at room-temperature, further investigations involving temperature variations are recommended to enhance the sensitivity and optimize the desorption dynamics.

In addition, variations in the resistance between the samples may arise from the natural variability of graphite-based materials. Therefore, further studies are required to improve the reproducibility and stability of these methods. Further studies should focus on optimizing the fabrication methods and exploring alternative dopant materials to enhance sensor performance.

CONCLUSION

This study demonstrates the successful fabrication and evaluation of a 2% Mn-doped Sri Lankan natural graphite thin-film sensor for the room-temperature detection of NH_3, C_3H_6O, and C_2H_5OH vapors. Structural analysis confirmed the incorporation of Mn into the graphite lattice, as evidenced

by the shift in the (002) XRD peak and the emergence of additional diffraction features associated with the Mn-related phases. The observed lattice distortion and induced strain suggest effective modification of the graphite structure, which plays a key role in enhancing the surface activity. SEM analysis further revealed a compact morphology with well-distributed Mn species and moderate porosity (~18.94%), providing sufficient active sites for gas adsorption. Gas sensing measurements showed that Mn doping significantly improved both the sensitivity and dynamic response compared to undoped natural graphite. Among the tested vapors, C_3H_6O exhibited the highest response, with the sensitivity increasing from 23.98% to 36.92%, accompanied by notably faster recovery behavior. Similar improvements were observed for NH_3 and C_2H_5OH, indicating that Mn incorporation enhances charge transfer interactions and increases the number of active adsorption sites on the graphite surface. Additionally, the reduced response and recovery times in the doped sensor confirmed improved adsorption-desorption kinetics, although partial baseline drift over repeated cycles suggested incomplete desorption of analyte molecules at room-temperature. Overall, the findings establish Mn-doped natural graphite as a promising, low-cost sensing material for the room-temperature detection of volatile organic compounds and NH_3. The enhanced performance is primarily attributed to the Mn-induced structural modification and increased surface reactivity. However, issues related to baseline recovery stability and cycle-to-cycle reproducibility indicate that further optimization of the doping concentration, film microstructure, and thermal treatment conditions are necessary. Future work should explore controlled defect engineering and temperature-assisted desorption strategies to further improve the sensor stability, selectivity, and long-term operational reliability.

Acknowledgement

The authors gratefully acknowledge Bogala Graphite Lanka PLC for providing the graphite samples used in this study. The authors also extend their sincere gratitude to Mr. Anura Liyanage and Mr. Saliya Gamlath for their invaluable assistance with this work.

REFERENCES

1. Lin PC, Villarreal R, Achilli S, Bana H, Nair MN, Tejeda A, et al. Doping graphene with substitutional Mn. ACS Nano. 2021;15(3):5449–5458. doi:10.1021/acsnano.1c00139. PMID:33596385.
2. Grotti M, Leardi R, Gnecco C, Frache R. Determination of manganese by graphite furnace atomic absorption spectrometry: Matrix effect control by multiple linear regression model. Spectrochim Acta B. 1999;54(5):845–851. doi:10.1016/S0584-8547(99)00027-0.
3. Lei Y, Butler D, Lucking MC, Zhang F, Xia T, Fujisawa K, et al. Single-atom doping of MoS2 with manganese enables ultrasensitive detection of dopamine: Experimental and computational approach. Sci Adv. 2020;6(32). doi:10.1126/sciadv.abc4250. PMID:32821846.
4. Wang W, Zhang Y, Shen C, Chai Y. Adsorption of CO molecules on doped graphene: A first-principles study. AIP Adv. 2016;6(2). doi:10.1063/1.4942491.
5. Karunasena IGPN, Rathnayake C, Thotagamuge R, Samarakoon SPAUK, Samarasekara P. Synthesis and characterization of thin film gas sensors using Sri Lankan natural graphite: comparative analysis of sensitivity to ammonia, acetone, and ethanol vapors. Ionic Res Eng J. 2026;9(7):2244-52. doi:10.64388/IREV9I7-1713855.
6. Mohammadi-Manesh E, Ahmadvand N, Rahmani S. Ag-doped monolayer and bilayer graphene for the gas sensor and purifier of industrial oils. Comput Theor Chem. 2023;1228:114274. doi:10.1016/j.comptc.2023.114274.
7. Gui Y, Peng X, Liu K, Ding Z. Adsorption of C2H2, CH_4 and CO on Mn-doped graphene: Atomic, electronic, and gas-sensing properties. Physica E Low Dimens Syst Nanostruct. 2020;119:113959. doi:10.1016/j.physe.2020.113959.
8. Song EH, Yan JM, Lian JS, Jiang Q. External electric field catalyzed N_2O decomposition on Mn-embedded graphene. J Phys Chem C. 2012;116(38):20342–20348. doi:10.1021/jp304757f.
9. Xie T, Tian C, Wang P, Zhao G. The adsorption behavior of gas molecules on Mn/N- and Mn-

doped graphene. Nanomaterials (Basel). 2024;14(16):1353. doi:10.3390/nano14161353. PMID:39195391.
10. Yi M, Shen Z, Zhang X, Ma S. Achieving concentrated graphene dispersions in water/acetone mixtures by the strategy of tailoring Hansen solubility parameters. J Phys D Appl Phys. 2013;46(2):025301. doi:10.1088/0022-3727/46/2/025301.
11. Jiang Z, Huang K, Yang D, Wang S, Zhong H, Jiang C. Facile preparation of Mn3O4 hollow microspheres via reduction of pentachloropyridine and their performance in lithium-ion batteries. RSC Adv. 2017;7(14):8264–8271. doi:10.1039/C6RA24803A.
12. Salvatore M, Carotenuto G, De Nicola S, Camerlingo C, Ambrogi V, Carfagna C. Synthesis and characterization of highly intercalated graphite bisulfate. Nanoscale Res Lett. 2017;12(1):167. doi:10.1186/s11671-017-1930-2. PMID:28274088.
13. Dahamni MA, Ghamnia M, Naceri SE, Fauquet C, Tonneau D, Pireaux JJ, et al. Spray pyrolysis synthesis of pure and Mg-doped manganese oxide thin films. Coatings. 2021;11(5):598. doi:10.3390/coatings11050598.
14. Barnakov CN, Khokhlova GP, Popova AN, Sozinov SA, Ismagilov ZR. XRD characterization of the structure of graphites and carbon materials obtained by the low-temperature graphitization of coal tar pitch. Eurasian Chem Technol J. 2015;17(2):87–93. doi:10.18321/ectj198.
15. Popova AN. Crystallographic analysis of graphite by X-ray diffraction. Coke Chem. 2017;60(9):361–365. doi:10.3103/S1068364X17090058.
16. Hassanzadeh-Tabrizi SA. Precise calculation of crystallite size of nanomaterials: A review. J Alloys Compd. 2023;968:171914. doi:10.1016/j.jallcom.2023.171914.
17. Chakraborthy A, Nuthalapati S, Nag A, Afsarimanesh N, Alahi MEE, Altinsoy ME. A critical review of the use of graphene-based gas sensors. Chemosensors. 2022;10(9):355. doi:10.3390/chemosensors10090355.

